3D seismic simulation of RC structures using damage mechanics: An assessment of merits and limitations

L. A. M. Mendes
Instituto de Engenharia de Estruturas, Território e Construção, Lisboa, Portugal.
Universidade da Madeira, Funchal, Portugal.

L. M. S. S. Castro
Instituto de Engenharia de Estruturas, Território e Construção, Lisboa, Portugal.
Instituto Superior Técnico, Universidade Técnica de Lisboa, Lisboa, Portugal.

E. P. M. F. Coelho
Laboratório Nacional de Engenharia Civil, Lisboa, Portugal.

SUMMARY:
This paper focus on assessing the use of continuum damage models for simulating the concrete response in refined three-dimensional seismic analyses on reinforced concrete (RC) structures.
This modelling strategy is validated in a series of case studies where the numerical response obtained is compared with experimental results from monotonic and cyclic quasi-static tests.
The paper ends with the conclusions extracted, in which the merits of this approach and the ability of reproducing the RC response with accuracy are clearly presented. On the other hand, the main drawbacks of this approach are also identified, in particular for high levels of inelasticity where the assumptions made in the models become far from the real response and thus this modelling strategy becomes inaccurate and unrealistic.

Keywords: Reinforced Concrete; Continuum Damage Mechanics; Seismic Response Simulation.

1. INTRODUCTION

The main objective of this paper is to assess the merits and limitations of using the *continuum damage mechanics* approach to simulate the concrete response in 3D seismic analyses using two case studies. These analyses are performed adopting the so-called local or refined modelling approach, in which the concrete domain is simulated using 3D elements and all the steel reinforcing bars in the RC member are included through their exact geometric distribution.

This modelling approach presents a great potential, making possible the direct simulation of complex phenomena like the three-dimensional strain and stress states in the concrete or the imperfect concrete-steel bond throughout the RC element. On the other hand, it requires the generation of complex and large meshes that invariably result in very large problem sizes. This leads to significant challenges, both in terms of the computation requirements (hardware) and in terms of the algorithms (software) required to perform the analysis. In addition, it is mandatory to adopt constitutive relations that are able to simulate the reversed cyclic response of the materials in order to perform dynamic seismic analyses, thus significantly increasing the complexity and the cost of the numerical model.

These requirements combined with the additional complexity of the formulation (e.g. the need for time integration algorithms) and supplementary input data (e.g. the need for earthquake records and mass distributions) has inhibited research and new developments in this modelling approach and the use of static non-linear models (e.g. the well-known pushover analysis) are usually preferred for design, assessment and even for seismic simulation of reinforced concrete structures.

In conclusion, this modelling technique presents significant challenges and still requires a significant research effort in order to be a practical and feasible simulation tool. Nevertheless, it presents a great potential that justifies a large development effort. A particular motivation for this research is to have a complementary, reliable and practical numerical tool that could be used to predict, follow and extend the expensive seismic tests being made in large-scale seismic test facilities (e.g. shaking table tests).

2. CASE STUDY 1: RC BEAM TEST BY BURNS AND SEISS

The authors Burns and Seiss (Burns and Seiss, 1962) performed static tests on 21 RC beams with different heights, compression reinforcement ratios, loading sequence and direction. This case study considers the specimen J-4, in which the beam does not have top longitudinal reinforcements and only two #8 bars ($\phi = 1$ in. $= 25.4$ mm) at the bottom. The stirrups are #3 bars ($\phi = 3/8$ in. $= 9.52$ mm) with 6 in. of spacing. A series of displacements is prescribed at the top face of the central top salience of the beam, which corresponds to point A in the model (see Fig. 2.1). Moreover, the vertical displacement is measured at the bottom face of the central bottom salience of the beam, which corresponds to point B in the model. Fig. 2.1 presents the finite element mesh adopted in the analyses. A total of 3264 square Q4 elements were considered for modelling the concrete ($b=h=1$ in.) using a continuum damage model and a plane stress hypothesis was adopted. The longitudinal reinforcements were modelled with 156 bar elements adopting an elastoplastic model and the stirrups were simulated by 26 elastic trusses. This discretization led to 7060 degrees-of-freedom plus one equation for imposing the displacement at point A using the Lagrange Multipliers technique (Cook et al., 1989).

The authors reported for specimen J-4 a concrete cylinder strength of 4.82 ksi (33.2 MPa) and a steel yield stress of 44.9 ksi (309.6 MPa). Information regarding the concrete mode I fracture energy was not reported by the authors. Lowes (Lowes, 1999) adopted $G_f^{\mathrm{I}} = 1.50$ lb/in. (262.7 N/m) to perform an energy-based regularization using a local damage model. This value seems excessive and after some tests, $g_f^{\mathrm{I}} = 1.05$ lb/in^2 (183.9 N/m^2) and $L_{nl} = 1.0$ in. were adopted and the *bell-shaped function*, as defined by Jirásek (Jirásek, 2002), was used for controlling the localization phenomenon. The monotonic constitutive relations adopted are presented in Fig. 2.2. More information about the material properties can be found in the report published by the authors (Burns and Seiss, 1962) and the complete list of the model parameters used can be retrieved in the work of Mendes (Mendes, 2011).

Seven analyses (Case #1 to #7) will be described to justify some of the choices made and the results obtained. The first four cases are characterized by the absence of stirrups and by the formulation used to model the concrete. In the first two cases (#1 and #2) the concrete is simulated using the original Mazars' model (Mazars, 1984). This model revealed a tendency to result in fragile materials ($g_f^{\mathrm{I}} < 0.5$ lbs/in.) by trying to match the tensile and compressive concrete resistance with realistic strains at peak stress. In the numerical simulations, these beams reached a nearly collapsed state at an early and unrealistic stage. These observations can be confirmed in the global force-displacement curves presented in Fig. 2.3 or in the damage distributions presented in Fig. 2.5. For cases #3 and #4 a modified version of the Mazars' model was used. In this formulation the tensile softening branch is linearized (see Fig. 2.2-a) making it easier to adjust the fracture energy density to values of about

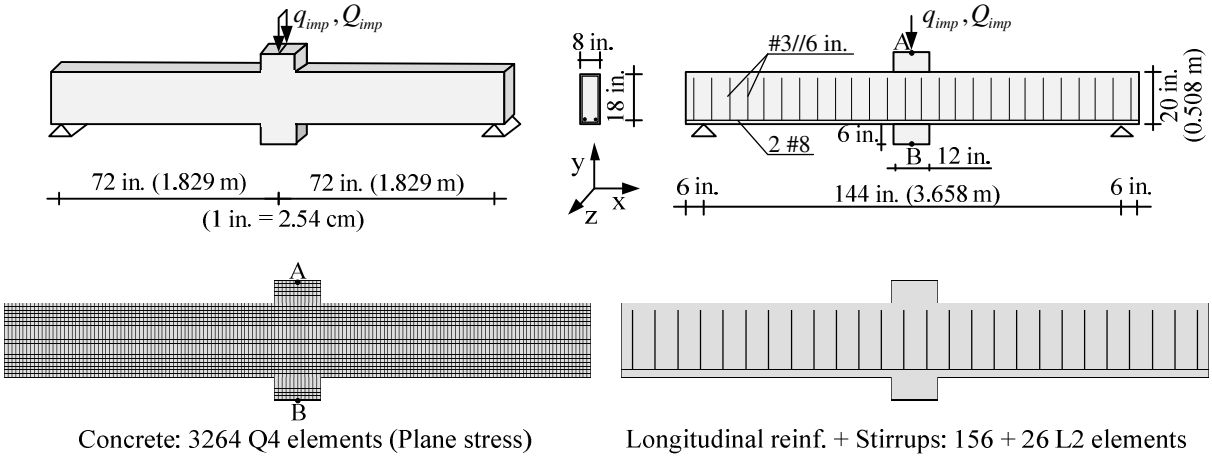

Figure 2.1. Definition of the problem and finite element mesh adopted.

$0.7 - 1.1$ lbs/in. The next step consisted in adding the beam stirrups to the simulation. This way, all the steel reinforcements are included in the analyses. This decision was made after observing the shear-like collapses in analyses #3 and #4. This change and some minor adjustments in the material properties lead to the best results obtained in this example (analyses #5 to #7).

The main difference between analyses #5 to #7 consists in not considering the resistance dispersion in the concrete for analysis #5. In the other two examples, a relative standard deviation of 18% was adopted for the tensile and compressive concrete resistance. This strength variation is implemented at the Gauss points level by generating pseudo-random numbers with a specific mean value and dispersion to simulate the material heterogeneity, see Mendes for more details (Mendes, 2011).

Analysis #5 revealed the tendency of the response to follow the symmetry of the beam, loading and boundary conditions. In the absence of softening, the response should present a perfect symmetric pattern. Nonetheless, the concrete presents softening branches that lead to localization, which is very sensitive to numerical accuracy variations and tend to destroy the symmetry by localization in one of the beam sides. This means that the response will tend to be very similar up to a certain point. Afterwards, the damage will present a tendency to concentrate in the most damaged zones, which consists in a limitation for the analyses because damage will tend to occur in similar positions. On the other hand, for the analyses #6 and #7, the response is asymmetric and much more variable because of the strength dispersion implemented. This randomness in the response can be clearly observed in Fig. 2.5 by noting the differences in the damage distributions and in the macro-cracks location.

Fig. 2.3 presents the global force-displacement curves obtained in the analyses, which are plotted against the experimental data obtained by Burns *et al.* (Burns and Seiss, 1962). For the analyses #5 to #7, it can be seen that the experimental and numerical curves are very close before the development of micro-cracking. On the other hand, the numerical curves are significantly above the experimental after cracking and up to yielding of the reinforcements. This difference is mainly due to three reasons. Firstly, the fracture energy of the concrete was increased in order to avoid the unrealistic shear collapses caused by considering an isotropic damage model, which penalizes the shear strength. Secondly, a residual concrete tensile strength of 3% was adopted to avoid having elements with no strength or stiffness (when the secant stiffness is adopted), in order to improve the numerical stability of the model. Finally, the experimental curve presents an unusual positive curvature between the cracking and yielding zones, which is associated with stiffness increase. This seems difficult to explain because the steel bars did not reach the strain-hardening plateau, not even yielding. In addition, the concrete tends to crack and decrease stiffness. Perhaps, the tests presented some additional source of flexibility that shifted to some extend the experimental curve. Nevertheless, a stiffer response in the numerical model is expected due to options taken to simulate the concrete.

In what concerns the numerical efficiency of the model, it was possible to observe a poor convergence rate in the iterations. To support this statement, Fig. 2.4 presents the number of iterations required by each time step to achieve convergence for the analysis #7. It can be seen that this number is high and with an average around 85-100 per load increment and with peaks when cracks are developing.

This behaviour is caused by the model used for simulating concrete because for most of the analysis the steel response is elastic. Using the secant stiffness for the concrete elements leads to poor convergence rates as this modulus can be very inefficient to find equilibrium.

3. CASE STUDY 2: RC PRECAST COLUMN TEST BY MENDES, COELHO AND COSTA

This case study illustrates the use of this combination of modelling techniques in the analysis of a 3D problem. For this purpose, the RC precast column shown in Fig. 3.1 was chosen, which was tested at LNEC by Mendes et al. (Mendes et al., 2006a, Mendes et al., 2006b, Mendes et al., 2007). These tests were carried out in the scope of the European Project “PRECAST - Seismic Behaviour of Precast Concrete Structures with Respect to Eurocode 8” and financed by the European Commission.

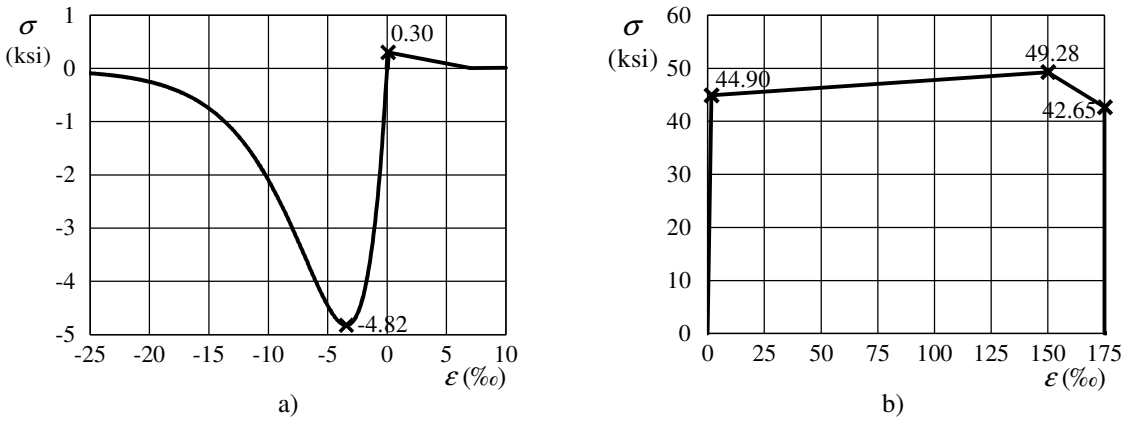

Figure 2.2. Constitutive relations: a) Concrete; b) Steel.

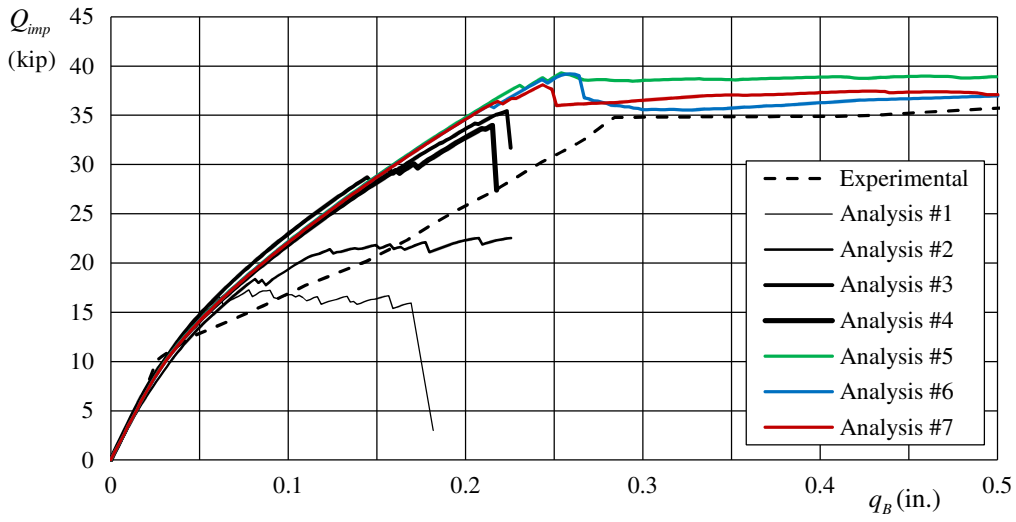

Figure 2.3. Global force-displacement curves.

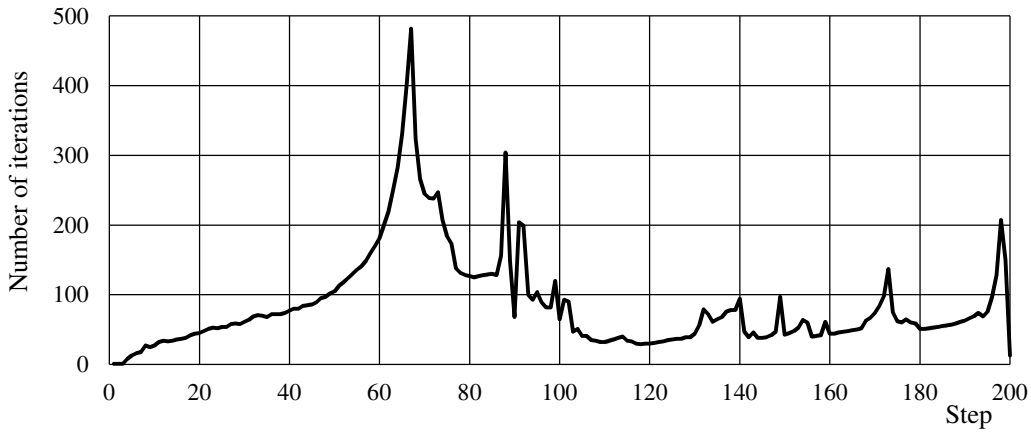

Figure 2.4. Analysis #7 – Number of iterations required to achieve convergence.

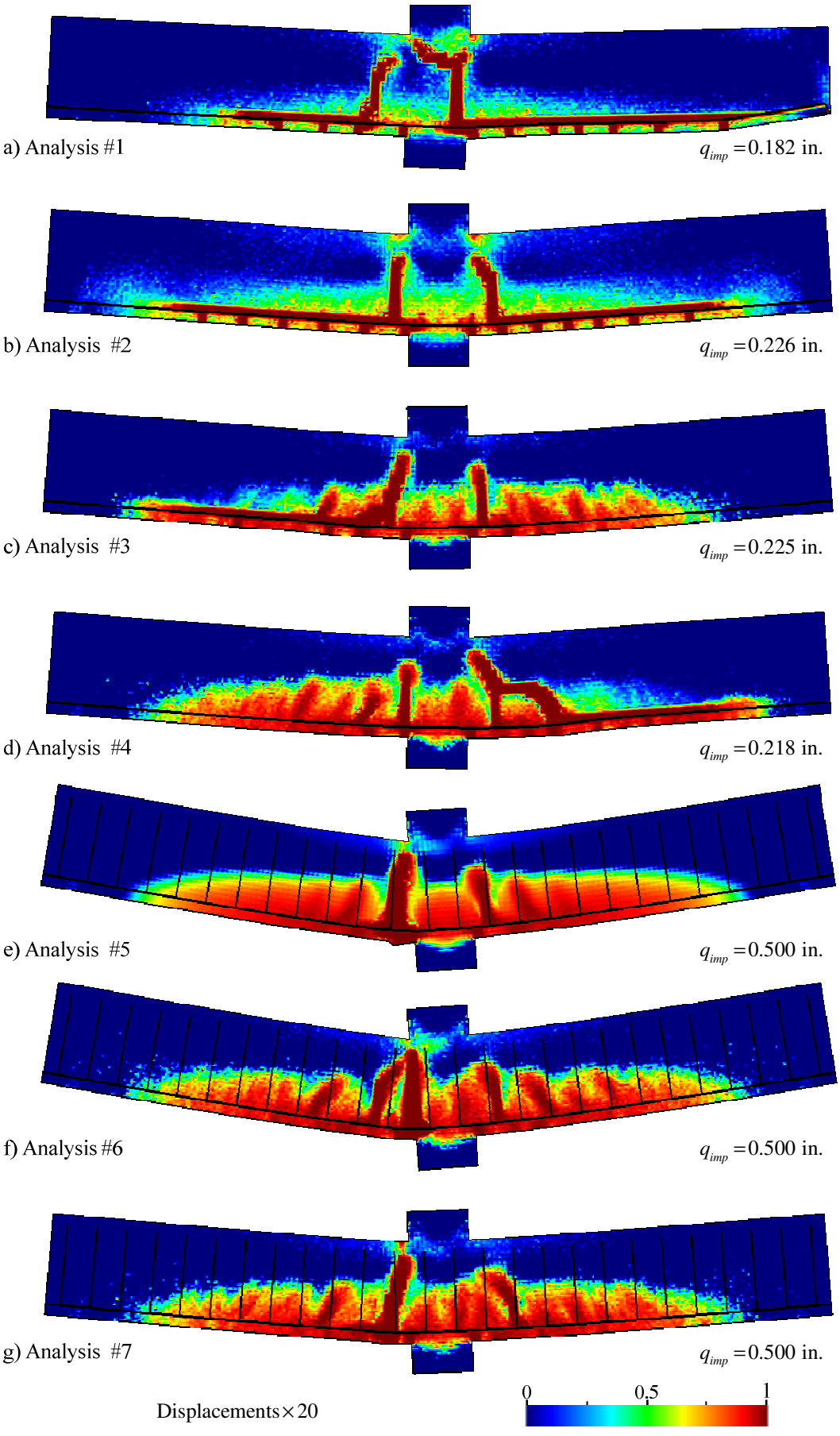

Figure 2.5. Deformed shape and damage distribution at selected time steps.

The experimental activity was divided in two phases. At first, a two-storey structure was tested using the triaxial shaking table. Afterwards, the structural response of the precast column-foundation and beam-column connections were characterized using quasi-static monotonic and cyclic tests. This example concentrates on the monotonic and cyclic tests executed on the socket-type column-foundation connections presented in Fig. 3.1-a. The footing and the column are precast and joined together in-situ by inserting the column into a pre-existing hole in the footing and by sealing them using a micro-mortar, as illustrated in Fig. 3.1-a. The tests were performed by prescribing displacements at the column top and a 15 mm diameter Dywidag bar placed in a hole inside the column was used to simulate typical levels of axial load, which was measured during the tests using a load cell. According to the authors, the precast connection performed very well and no significant damage was identified in this element. In fact, almost all the visible damage was distributed in the span of the columns and the response was typical of a cast in-situ RC member.

Two meshes were used to perform the analyses. For the cyclic test simulation described ahead, it was used a uniform structured mesh with 1136 cubic hexahedrons with 2.5 cm edge and 160 bar elements 2.5 cm long for the longitudinal reinforcements and 10.0 cm for the stirrups. On the other hand, for the monotonic test simulation the hexahedron-size along direction *x* is reduced to 1.25 cm (see Fig. 3.3), as this experiment reached higher inelasticity levels, which required a more refined mesh. Both meshes adopt what is called a *Hybrid Discretization* to decrease the number of unknowns in the simulation by using a simplified mesh in the zones expected to remain elastic or with minor nonlinear effects, see Mendes for more details (Mendes, 2011). The transition between the refined and simplified parts of the mesh is executed using kinematic constraints enforced by Lagrange Multipliers.

The concrete was simulated with the nonlocal modified version of the *Mazars'* model mentioned before and the longitudinal reinforcements with Euler-Bernoulli beam-column elements defined by an elastoplastic relation for the axial component and elastic in all remaining directions. The latter modelling approach was used to add lateral resistance to the RC member and to reduce the risk of unrealistic shear failures associated with the isotropic damage model used for concrete. The stirrups were considered elastic during the analyses.

In what concerns the concrete, a Eurocode 2 (CEN, 2001) C35/45 concrete class was adopted. The adopted uniaxial stress-strain relation is presented in Fig. 3.2-a and the tensile strength dispersion was considered by adopting 18% of relative standard deviation and 2/3 of this value (12%) for the compressive strength. Regarding the reinforcing steel, the A500NR steel class was adopted and the mechanical parameters used are: $E_s = 200$ GPa, $\sigma_{sy} = 585$ MPa, $\varepsilon_{su} = 9.4\%$, $\beta_0 = 0.51\%$ (Fig. 3.2-b). The complete list of the model parameters adopted can be obtained in the work of Mendes (Mendes, 2011).

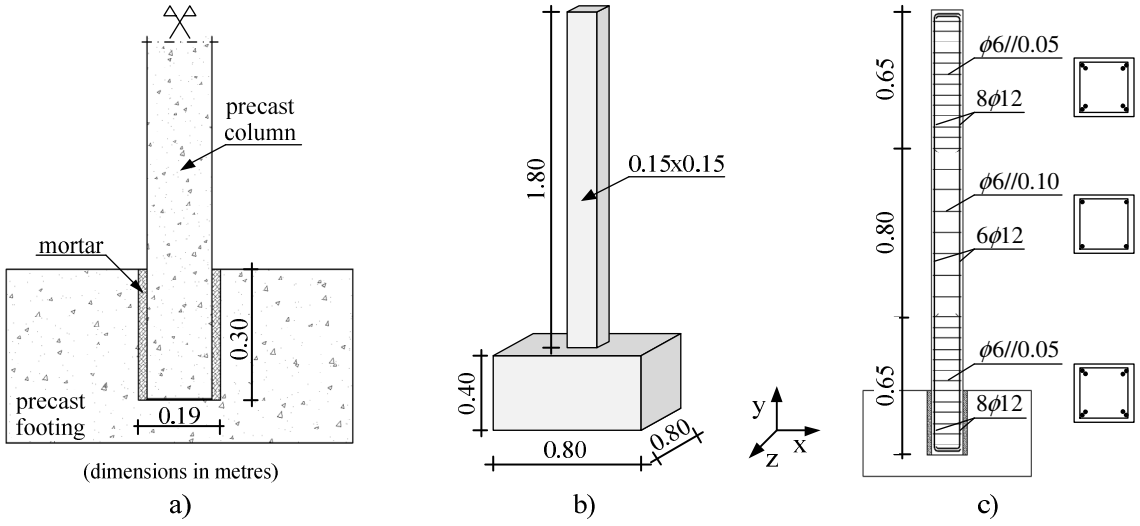

Figure 3.1. Example RC4– Definition of the problem.

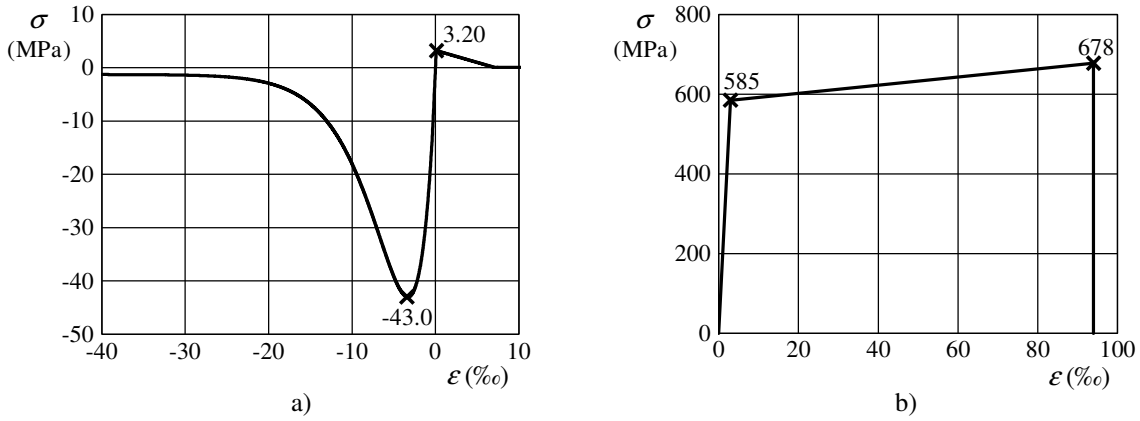

Figure 3.2. Constitutive relations: a) Concrete; b) Steel.

3.1. Monotonic test

The first analysis was performed by imposing a monotonic quasi-static lateral displacement 1.50 m above the footing top. This test layout follows the experiment performed by Mendes et al. (Mendes et al., 2007) with specimen P1.

Fig. 3.3 presents the most relevant results to characterize the concrete response throughout the analysis, namely the Mazars' combined damage variable distribution, the principal strains, and the principal stresses, all presented on the deformed configuration. It can be seen that initially the damage concentrates mainly in the tensioned part of the column, making possible the simulation of the distributed micro-cracking along the member. Afterwards, the damage starts to concentrate between 0.30 m and 0.35 m above the footing top, precisely in the same position where half of the reinforcements are removed (see Fig. 3.4-b). Subsequently, the most damaged zone spreads to a wider region and the column deformations tend to concentrate into the macro-crack and the rest of the bar presents reduced deformations. Furthermore, a clear tendency of the macro-crack to become diagonal along the x direction can be identified (see Fig. 3.3). Additionally, the longitudinal reinforcements showed strain levels reaching up to 2% and stress values of about 600 MPa. It can be concluded that these bars achieved yielding during the simulation, hence working already in the strain-hardening branch. On the other hand, the stresses on the stirrups were below ±100 MPa for all time steps and the maximum stresses were reached near the macro-crack zone.

Fig. 3.6 presents the force *vs.* prescribed displacement curve plotted against the experimental curve obtained by Mendes *et al.* (Mendes et al., 2007). The first aspect that is visible in this figure is that the numerical model using this discretization was not able to follow the entire experimental curve, although yielding of the reinforcements can be clearly identified. This is certainly related to the high inelasticity level concentrated in the macro-crack, for which the continuum damage approach becomes unrealistic and presents convergence problems. As before, the average number of iterations was relatively high (up to 160), which demonstrates the model inefficiency for high inelasticity levels.

The global force-displacement curve presented in Fig. 3.6 has some similarities with the one obtained in the previous case study (see Fig. 2.3). Namely, the initial stiffness is simulated with good accuracy using typical material parameters for defining the constitutive models. Furthermore, after concrete cracking and up to steel yielding the global response curve is stiffer than the experimental one. Once again, this can be related to the use of high mode I fracture energy density in the concrete model ($g_f^1 = 11286\ \mathrm{N/m^2}$, $L_{nl} = 2.0$ cm). As before, this is done to avoid premature and unrealistic shear-type collapses caused mainly by the isotropic damage formulations adopted. In this case the difference was smaller than the one observed in the previous case. After steel yielding, the numerical and experimental curves converge and remain very close in most of the post-yielding branch.

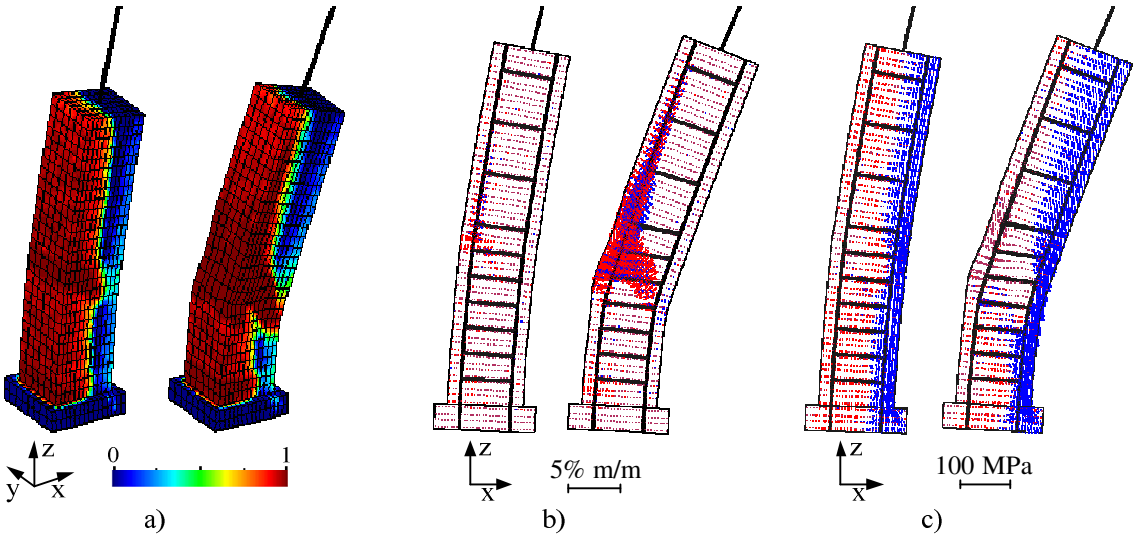

Figure 3.3. Structural response of the concrete at q_{imp} ={3.0;5.8} cm : a) Damage distributions; b) Principal strains; c) Principal stresses (displacements x10).

Figure 3.4. Monotonic test with specimen P1 performed by Mendes *et al.* (Mendes et al., 2007): a) test under execution; b) inspection made to the reinforcements after the test.

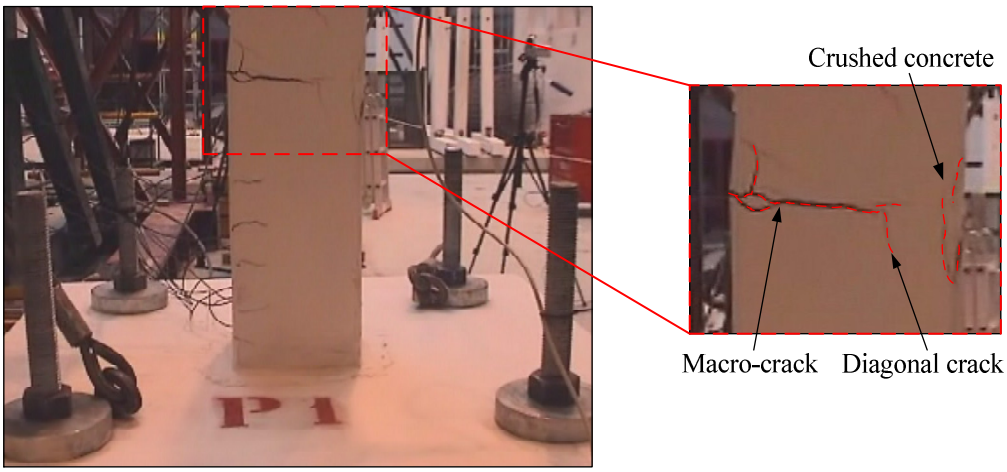

Figure 3.5. Cracking pattern observed on specimen P1 by Mendes *et al.* (Mendes et al., 2007).

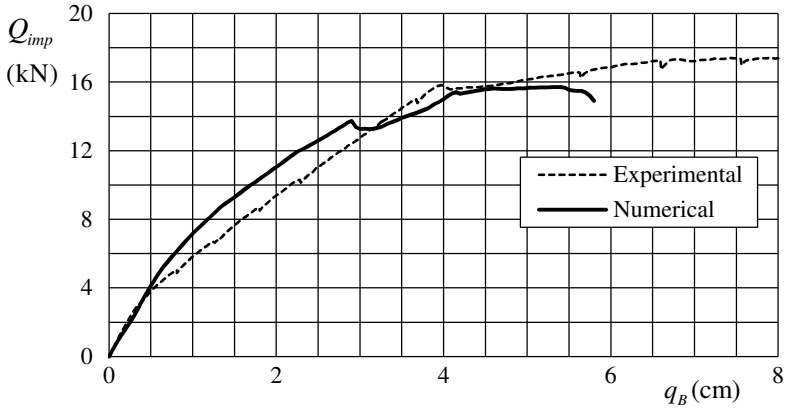

Figure 3.6. Global force-displacement curves.

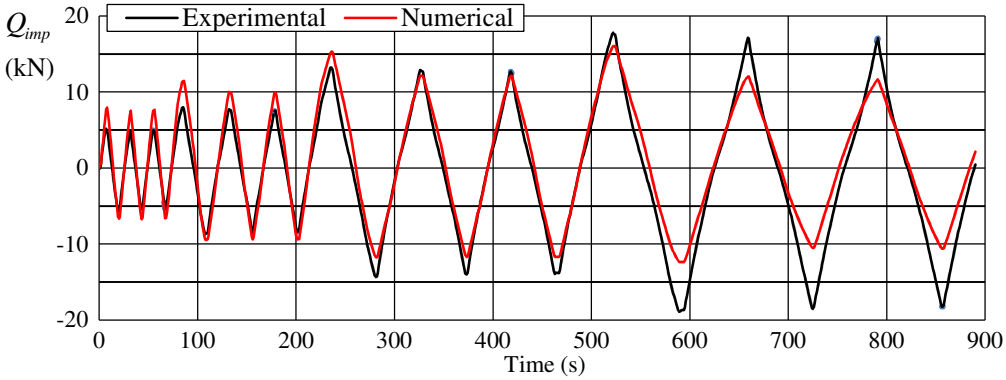

Figure 3.7. Cyclic test - Evolution in time of the force associated with the prescribed displacement.

Fig. 3.4-a presents a general view of the experiments in progress where it can be easily seen that the deformation tends to concentrate at about 0.35 m from the footing top, as reported by Mendes et al. (Mendes et al., 2007). Moreover, Fig. 3.4-b presents a detail of the P1 specimen after the test and after removing the cover concrete. The authors found that the macro-crack opened exactly in the region where half of the reinforcements are interrupted. Furthermore, Fig. 3.5 presents a detail of the macro-crack zone during the test, which illustrates the cracking pattern in the column. Bending cracks in the tensioned side of the column can be easily observed. In addition, it can be identified that a macro-crack is clearly opened on the tensioned side of the column and that the concrete starts to be crushed in the compressed face. Another interesting aspect to be noticed is that the same diagonal crack observed in the numerical model can be also detected in the images from the experiments. The tendency to generate this diagonal crack can be associated with perturbations in the stress fields in the transition zone between four and eight longitudinal reinforcements.

3.2. Cyclic test

This analysis was performed to test the models under cyclic and alternating loading. The cyclic test with specimen P4, executed in the scope of the same testing programme, was used as the reference for this computation. It should be emphasized that the loading point was repositioned at 1.375 m above the footing top and the loading time history follows the experimental, which includes a series of 3 complete cycles with amplitude of ±0.54, ±1.07, ±2.16 and ±3.23 cm (Mendes et al., 2007).

Fig. 3.7 presents the force vs. prescribed displacement curve plotted against the experimental results obtained by Mendes et al. (Mendes et al., 2007). It can be seen that the experimental cycles are reasonably followed by the numerical model. Nonetheless, it can be observed that the numerical curve presents a higher stiffness in the first series of cycles (amplitudes of ±0.54 and ±1.07 cm). The cycles with amplitude ±2.16 cm are the most similar with the experimental results, and for the largest amplitude cycles (±3.23 cm), the numerical results reveal higher strength degradation and the

differences become more significant. This can be related to the fact that for this load level the response is already significantly inelastic. Hence, the continuum damage approach becomes less realistic.

The average number of iterations required to achieve convergence decreased significantly by comparing these results with the ones from the previous analysis. This can be related to the fact that the branches associated with unloading or reloading until a previous load level tend not to generate new damage. Therefore, the convergence is easier and faster. Nevertheless, additional convergence difficulties were observed when the concrete elements changed from tension to compression and vice-versa, due to the use of two independent damage variables in the Mazars' model.

4. CONCLUSIONS

The constitutive model adopted for the concrete is based on the *continuum damage mechanics* (CDM) approach and adopts a smeared simulation of cracking and can capture many aspects of the concrete response. In the case studies presented in this paper, the CDM approach proved to be adequate for simulating the initial diffuse cracking. The main problems arise for intense nonlinear response involving opening of macro-cracks. In those situations, the convergence is very slow and unrealistic collapses can occur due to the approximations adopted in the models, in particular, the isotropic damage formulation. The adopted solution to mitigate this problem was to increase the mode I tensile fracture energy and to add residual strength levels to the concrete. This resulted in higher stiffness and resistance. Nevertheless, the development of macro-cracks was possible to be simulated with an interesting accuracy, considering the implicit approximation in the smeared crack approach for modelling the concrete fracture.

Under reversed loading, it was possible to identify convergence difficulties when loading is made after severe damage in the opposite direction. This is related to the use of damage models with two independent damage variables (e.g. Mazars' model). Furthermore, the use of a secant stiffness proved to be a robust approach, but the convergence rate was very poor, leading to a large number of iterations to achieve convergence for the time steps associated with high inelasticity.

As a conclusion, it is possible to stress that concrete modelling with three-dimensional refined meshes still requires a large research effort, in order to have a practical and robust model that can produce accurate and realistic results under general loading cases. The combination of the CDM approach for the initial diffuse micro-cracking with another technique for modelling the response of fully open macro-cracks (e.g. enriched finite elements with embedded cracks) seems to be a feasible approach.

REFERENCES

Burns, N. H. & Seiss, C. P. 1962. Load-Deformation Characteristics of Beam-Column Connections in Reinforced Concrete. Civil Engineering Studies, Structural Research Series No. 234. University of Illinois.

CEN 2001. Eurocode 2: Design of concrete structures. Part 1: General rules and rules for buildings. In: Comité Européen de Normalisation (ed.) 2nd draft ed. Brussels.

Cook, R. D., Malkus, D. S. & Plesha, M. E. 1989. Concepts and Applications of Finite Element Analysis, New York, John Wiley & Sons, Inc.

Jirásek, M. 2002. Objective modeling of strain localization. Revue Française de Génie Civil, 6, 1119-1132.

Lowes, L. N. 1999. Finite element modeling of reinforced concrete beam-column bridge connections. PhD Thesis, University of California.

Mazars, J. 1984. Application de la mécanique de l'endommagement au comportement non linéaire et à la rupture du béton de structure. PhD Thesis, Université Paris VI.

Mendes, L., Coelho, E. & Campos Costa, A. Seismic Tests of a RC Precast Building System. 1st European Conference on Earthquake Engineering and Seismology, 2006a 3-8 September, Geneva, Switzerland.

Mendes, L., Coelho, E. & Costa, A. C. 2006b. Shaking Table Tests of a Reinforced Concrete Precast Building System. Relatório nº97/2006 - NESDE. Lisboa: Laboratório Nacional de Engenharia Civil.

Mendes, L., Coelho, E. & Costa, A. C. 2007. Cyclic Tests of Joints from a Reinforced Concrete Precast Building System. Relatório nº30/2007 - NESDE. Lisboa: Laboratório Nacional de Engenharia Civil.

Mendes, L. A. M. 2011. Refined Three-dimensional Seismic Analysis of Reinforced Concrete Structures. Ph.D. in Civil Engineering, Instituto Superior Técnico, Universidade Técnica de Lisboa.